Compact cryogenic self-aligning fiber-to-detector coupling with losses below one percent

Aaron J. Miller,[1,*] **Adriana E. Lita,**[2] **Brice Calkins,**[2] **Igor Vayshenker,**[2] **Steven M. Gruber,**[2] **Sae Woo Nam**[2]

[1]*Department of Physics, Albion College, Albion, Michigan, USA*
[2]*National Institute of Standards and Technology, Boulder, Colorado, USA*

[*]*ajmiller@albion.edu*

Abstract: We present a compact packaging technique for coupling light from a single-mode telecommunication fiber to cryogenic single-photon sensitive devices. Our single-photon detectors are superconducting transition-edge sensors (TESs) with a collection area only a factor of a few larger than the area of the fiber core which presents significant challenges to low-loss fiber-to-detector coupling. The coupling method presented here has low loss, cryogenic compatibility, easy and reproducible assembly and low component cost. The system efficiency of the packaged single-photon counting detectors is verified by the "triplet method" of power-source calibration along with the "multiple attenuator" method that produces a calibrated single-photon flux. These calibration techniques, when used in combination with through-wafer imaging and fiber back-reflection measurements, give us confidence that we have achieved coupling losses below 1 % for all devices packaged according to the self-alignment method presented in this paper.

OCIS codes: (220.1140) Alignment; (060.2380) Fiber optics sources and detectors.

References and links

1. E. Knill, R. Laflamme, and G. J. Milburn, "A scheme for efficient quantum computation with linear optics," Nature **409**, 46–52 (2001).
2. M. Varnava, D. E. Browne, and T. Rudolph, "How good must single photon sources and detectors be for efficient linear optical quantum computation?" Phys. Rev. Lett. **100**, 060502 (2008).
3. A. J. Miller, S. Nam, J. M. Martinis, and A. V. Sergienko, "Demonstration of a low-noise near-infrared photon counter with multiphoton discrimination," Appl. Phys. Lett. **83**, 791 – 793 (2003).
4. A. E. Lita, A. J. Miller, and S. Nam, "Counting near-infrared single-photons with 95% efficiency," Opt. Exp. **16**, 3032–3040 (2008).
5. D. Rosenberg, A. E. Lita, A. J. Miller, and S. Nam, "Noise-free high-efficiency photon-number-resolving detectors," Phys. Rev. A **71**, 61803 (2005).
6. T. Gerrits, S. Glancy, T. S. Clement, B. Calkins, A. E. Lita, A. J. Miller, A. L. Migdall, S. Nam, R. P. Mirin, and E. Knill, "Generation of optical coherent state superpositions by number-resolved photon subtraction from squeezed vacuum," Phys. Rev. A **82**, 031802 (2010).
7. A. E. Lita, B. Calkins, L. A. Pellouchoud, A. J. Miller, and S. Nam, "Superconducting transition-edge sensors optimized for high-efficiency photon-number resolving detectors," Proc. SPIE **7681**, 76810D–1–10 (2010).
8. J. H. Lehman and X. Li, "A transfer standard for optical fiber power metrology," Appl. Opt. **38**, 7164–7166 (1999).
9. I. Vayshenker, S. Yang, X. Li, T. R. Scott, and C. L. Cromer, "Optical fiber power meter nonlinearity calibrations at NIST," NIST Special Publication 250-56 (2000).

#143645 - $15.00 USD
Received 8 Mar 2011; accepted 25 Mar 2011; published 25 Apr 2011

1. Introduction

In fiber-coupled optoelectronic systems, source-to-fiber and fiber-to-detector coupling of light has been traditionally important for reducing optical losses. However, recent emerging applications of quantum optical systems have placed increasingly stringent requirements on these coupling connections [1,2]. Theoretical and experimental progress in these fields has motivated the development of extremely high-efficiency single-photon optical systems, including sources, optics, and detectors. In this paper we present the design, fabrication, and demonstration of a fiber-to-detector coupling technique that exhibits low loss, cryogenic compatibility, easy and reproducible assembly, and results in a compact assembled package with low component cost.

Our method exploits the micrometer resolution of photolithographic processes to etch the outer edges of a device-bearing silicon substrate. The substrate is micromachined into a circular shape to a precision of approximately one micrometer in diameter. We then leverage the commercially available high-tolerance fiber-alignment components ubiquitous in the telecommunication industry to align a ferrule-terminated single-mode fiber to the center of the circular substrate. By ensuring our optical photon-counting device is centered on the circular substrate, we easily achieve alignment accuracy comparable to, or exceeding, the best attained by manual alignment under a microscope by use of micromanipulators or micrometer stages.

The impetus to develop new fiber-to-detector coupling comes from the high performance of our existing superconducting transition-edge sensors (TESs) used for number-resolved single-photon counting [3]. As the device quantum efficiency (QE) of the TES devices has approached 100 % [4], the few-percent losses from system components must be eliminated for the full benefit of the ultra-high device efficiency to be available for science applications. Additionally, because our devices require sub-Kelvin cryogenic operation, we have additional challenging engineering requirements. Our goals for this coupling method are as follows: (1) losses below 1 %, (2) sub-Kelvin operating temperatures, (3) no moving parts at low temperature, (4) fast assembly with no manual alignment, (5) compact packaging to enable many detectors in limited cryogenic volume, and (6) exploit low-cost commercial, off-the-shelf components as much as possible.

Prior to implementation of the "self-alignment" method presented in this paper, manual alignment of devices has resulted in fiber-to-detector coupling above 85 %, with some approaching 100 % [4–6]. However, this manual method of alignment had significant drawbacks: 1) alignment required manipulation of device mounts under a microscope by use of micrometer-resolution movement stages, 2) the alignment process took approximately 30 minutes per device by a skilled operator, 3) the cryogenic device package required careful material selection, mechanical design, and machining to minimize losses from thermal-contraction-induced alignment errors, 4) substrate thickness and machined component measurements were made on each device and machined package to ensure that the distance between the fiber tip and the device was sufficient to allow for the thermal contraction of the entire assembly to prevent catastrophic damage to the detectors, and 5) the manual alignment process and subsequent assembly yielded a coupling efficiency above 85 % for only about one quarter of the devices, when tested cryogenically.

2. Fiber-to-detector self-alignment

Figure 1 shows the components and completed assembly for the design presented here. The fiber coupling consists of four critical alignment components, enumerated by the labels given in Fig. 1:a standard telecommunication single-mode-fiber (SMF) terminated by a zirconia ferrule, (b) zirconia alignment sleeve, (c), (d), (e) the custom micromachined device substrate, and a custom back-side zirconia or sapphire substrate ferrule. This technique allows the detector (typically 25 μm×25 μm) to be placed in the middle of a micromachined Si disk that has

#143645 - $15.00 USD Received 8 Mar 2011; accepted 25 Mar 2011; published 25 Apr 2011

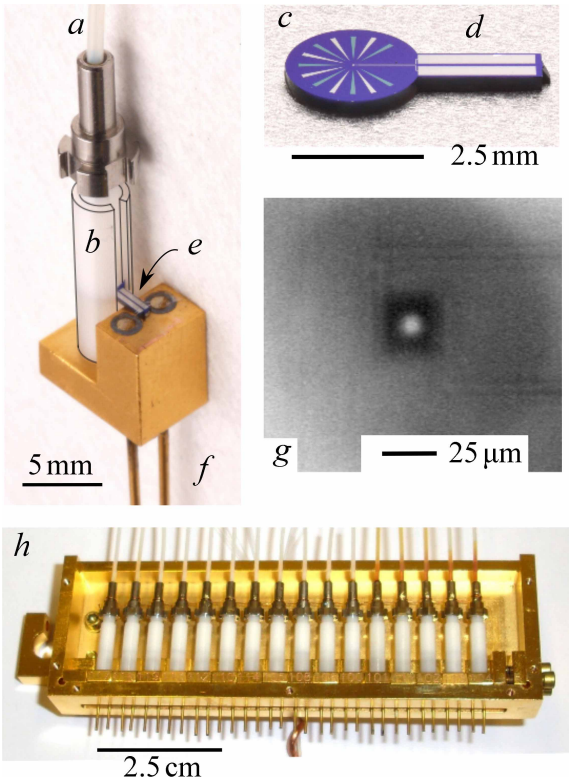

Fig. 1. Complete fiber-to-detector assembly showing (a) single-mode fiber terminated in a stainless steel and zirconia ferrule inserted into (b) a zirconia alignment sleeve (outlined for clarity). The completed detector and substrate (c) has wiring along a silicon "tongue" (d) that extends out the zirconia sleeve (e) and is wirebonded to pins (f) that allow electrical connection to cryogenic pre-amplifiers. A fully assembled device viewed via through-wafer infrared imaging showing (g) the laser light (bright) centered on the 25 µm×25 µm square device (dark square). A complete cryogenic assembly (h) containing 16 self-aligned, fiber-coupled photon-number-resolving devices.

a diameter slightly less than the inner diameter of a telecommunications fiber ferrule sleeve. The precise dimensions of the standard fiber ferrule sleeve makes possible the alignment of the ~9 µm diameter core of the fiber to the high-QE detector. Self-alignment is ensured by the precise dimensions of circular chips, fiber ferrule and ceramic alignment sleeve. The use of zirconia ceramic ferrules and sleeves is standard in the telecommunications industry and results in sub-micrometer center-to-center lateral alignment between opposing ferrules.

The circular silicon substrate is patterned by use of the standard semiconductor photolithography processes. The silicon is then micromachined with a standard Bosch dry-etch process that provides a near-vertical etch profile through the 275 µm thick Si wafer. For this thickness of substrate we observe approximately 1 µm of undercut around the circular edges of the 2.5 mm-diameter substrates. During the long-duration through-wafer etch, the photoresist gets slowly etched as well. Consequently, a photoresist of thickness 7 µm is required to protect the top-side wiring and devices from etch-induced damage. All processing steps (e.g., photoresist baking, wafer mounting on carrier wafer, and lateral etch, etching time based on silicon substrate thickness) are carefully characterized to ensure that the cumulative variability in the

#143645 - $15.00 USD
Received 8 Mar 2011; accepted 25 Mar 2011; published 25 Apr 2011

photoresist reflow, developing undercut, and etch undercut are designed to achieve the final substrate diameter of (2.497±0.001) mm, targeted at an outer diameter 3 μm smaller than the inner diameter of the alignment sleeve to allow for damage-free assembly.

Our circular substrates have an integrated Si beam (or "tongue") that extends through the ceramic alignment sleeve, as seen in Fig. 1(e). The opening of the sleeve is specified to be 1 mm wide to accommodate the 800 μm wide Si beam that carries the detector wiring out through the slot to enable wirebonding to the machined metal substrate holder, as seen in Fig. 1(e). The back-side ferrule is press-fit into a machined hole to capture the ferrule and to provide thermal connection between the zirconia components and the cooled metal components. It is important for the cryogenic compatibility that the ferrule-sleeve-substrate-ferrule assembly is attached to the cryostat at only one end. As the assembly is cooled from room temperature to below 1 K the single-end connection enables the assembly to thermally contract without introducing appreciable displacement between the zirconia components and the silicon substrate. Such displacement may induce coupling losses or, at worst, physical detector damage.

To insert the circular substrate into the alignment sleeve, a blank (non-fiber-containing) ferrule is first inserted into the alignment sleeve to spread the sleeve open. The circular substrate is placed on the backing ferrule and the alignment sleeve is slid over the device and backing ferrule. The blank ferrule is then removed. At the time of assembly into the cryostat, a fiber-containing ferrule is then slid into the alignment sleeve until the fiber is touching the substrate and the aligned device package is mounted into a mechanical enclosure with many other device packages, seen in Fig. 1(h), to be mounted in the cryostat. The individual device package assembly process is faster than performing manual alignment (under 5 minutes per device compared to 30 minutes) and requires neither the use of a microscope, nor custom micromanipulators or micrometer-resolution movement stages. The critical alignment is accomplished by use of the high-precision, low-cost zirconia fiber-alignment components common to the telecommunication industry. Once assembled, the self-alignment detector package has a volume of approximately 0.3 cm^3, enabling three times the number of packaged devices to fit into the same volume as a single manually aligned package under our previous design.

3. Alignment verification

To determine the effectiveness of this coupling scheme, the backing ferrule was replaced by a glass cylinder with dimensions matching the ferrule. Laser light of 1550 nm wavelength wavelength was sent into the fiber and images of the transmission of the laser light through a device and through the substrate were acquired with an infrared camera; an example image is shown in Fig. 1(g). The location of the centroid of the laser spot was recorded relative to the device geometry. In the image, the device is a thin (20 nm thick) tungsten square of 25 μm×25 μm. Measurements from the independent assembly of 35 such aligned devices resulted in the distribution of offset errors shown in Fig. 2. Also shown is the best-fit normal distribution with a mean offset error of 3.1 μm. This non-zero offset is consistent with the designed 3 μm undersizing of the substrate diameter relative to the inner diameter of the zirconia alignment sleeve. Assuming the fiber mode is Gaussian with a mode-field diameter of 10 μm and a 25 μm×25 μm square detector, an alignment error of 3 μm is calculated to result in a decrease in coupling efficiency of less than 0.1 %.

A second indication that the alignment is sufficient to place the fiber over our devices is the measured back-reflection from the fiber-coupled device. Figure 3 shows the less than 1 % absolute reflectivity from seven independently assembled self-aligned fiber-coupled devices across the C and L telecommunication bands (1525–1630 nm). Each device was illuminated with a tunable laser source and the reflected power was measured by use of a fiber circulator. The resulting back-reflected power was calibrated relative to the known 3.6 % reflection from

#143645 - $15.00 USD Received 8 Mar 2011; accepted 25 Mar 2011; published 25 Apr 2011

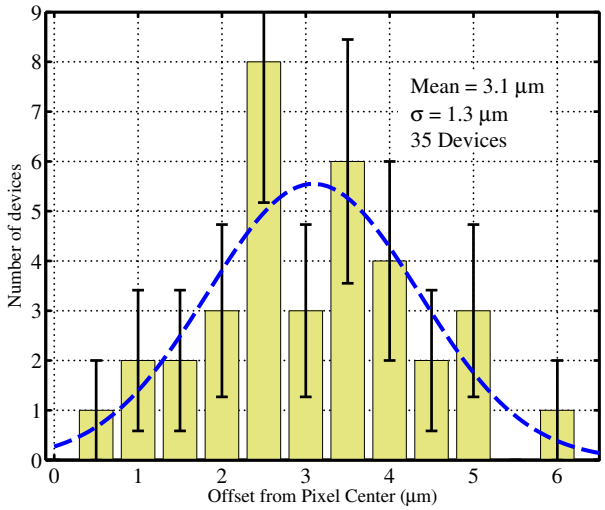

Fig. 2. Result of the measurement of the alignment error from 35 assembled transition-edge sensor photon counters by use of the self-aligning fiber-to-detector method. The average radial displacement was ~3 µm, consistent with the intentional 3 µm substrate undersizing.

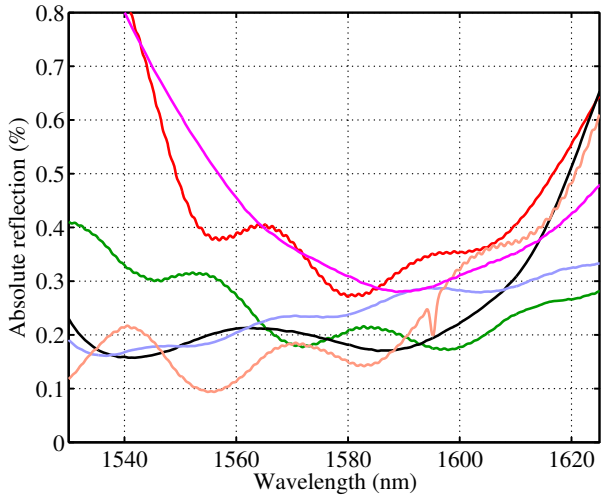

Fig. 3. Absolute reflectance of eight fiber-coupled devices with maximum absorption at a wavelength near 1580 nm. Reflectance was measured via fiber back-reflection at room temperature.

#143645 - $15.00 USD
Received 8 Mar 2011; accepted 25 Mar 2011; published 25 Apr 2011

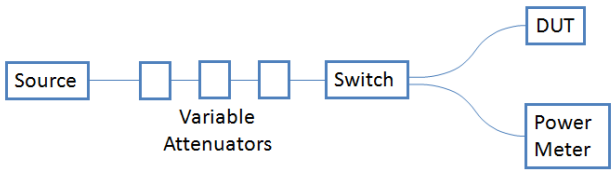

Fig. 4. Multiple-attenuator method for measuring the single-photon detection efficiency of a device under test (DUT).

an unterminated flat-polished fiber. All devices came from a single fabricated wafer in which the device structure was independently measured by use of an optical reflectometer to have a reflectivity of less than 1 % at these wavelengths. The reflection is seen to be consistently very low for the assembled package, giving confidence that the fiber end is well coupled to the highly absorbing detectors.

4. Detector calibration at the single-photon level

The effectiveness of this alignment technique at cryogenic temperatures can be demonstrated by measurements of single-photon system detection efficiency of the aligned devices when they are operating at low temperature ($<$1 K). System detection efficiency can be given as

$$\eta_{\text{system}} = \eta_{\text{fiber}}\eta_{\text{coupling}}\eta_{\text{absorption}}\eta_{\text{QE}}\eta_{\text{trigger}},$$

where η_{fiber} accounts for losses in the optical fiber system between the (room-temperature) light input point and the (cold) detector, η_{coupling} accounts for overlap between the optical mode in the fiber and the detector itself, $\eta_{\text{absorption}}$ is the fraction of the power incident on the device that is absorbed, η_{QE} is the fraction of absorbed photons that result in an electrical signal (pulse) at the detector readout, and η_{trigger} is the fraction of electrical pulses that meet the signal processing trigger criteria and are ultimately counted. For optical TES devices embedded in an optical cavity, $\eta_{\text{absorption}}$ should be near unity [4, 7]. The factor η_{QE} is unity because an absorbed photon must produce an increase in the temperature of the superconducting thermometer. For high signal-to-noise and pulsed operation as in this work, η_{trigger} is near unity, however this factor could be less than unity in cases of high CW count rates or low signal-to-noise on photon events. We expect that all losses are small relative to coupling losses and a measurement of system detection efficiency is a reasonable proxy for a measurement of coupling efficiency.

Currently there does not exist a calibrated single-photon source. As a result, measurements of the detection efficiency of a single-photon detector must rely on a calibrated optical power source, combined with a series of carefully measured linear optical attenuators. One way of doing this measurement is diagrammed in Fig. 4. In order for this setup to work, the optical attenuators must be switchable, repeatable, and linear, and the power meter must be calibrated at a variety of input power levels. The total dynamic range of the power meter calibration determines the attenuation that can be applied by each attenuator, and the output power of the source then determines the number of attenuators that must be used. When all attenuators are activated, the result is an indirectly calibrated single-photon source. The dominant uncertainty in this calibration is a multiple (in this case, three) of the systematic error in the calibration of the power meter. In practice, the calibration of the optical power meter comes in two parts. First, the power meter response is compared to a transfer standard detector at the wavelength of interest, and at a given input power level [8]. In our case this calibration was done by the

#143645 - $15.00 USD Received 8 Mar 2011; accepted 25 Mar 2011; published 25 Apr 2011

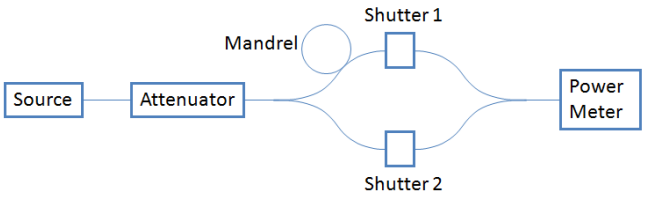

Fig. 5. Setup for power meter nonlinearity calibration. Power measurement V_1 is taken with shutter 2 closed, V_2 is taken with shutter 1 closed, and V_3 is taken with both shutters open. The extra mandrel of optical fiber is chosen so that the path difference is much longer than the coherence length of the source. Comparing the three measurements at a given power level indicates the local nonlinearity of the power meter.

optical fiber power metrology group at NIST, Boulder Colorado. Secondly, the linearity of the power meter response is measured relative to the calibration power level by means of a series of additive power measurements [9]. The setup for this linearity calibration is shown in Fig. 5, and is known as a triplet measurement. By comparing the power measured from each of the two beamsplitter arms alone to the power measured when the two arms are combined, it is possible to determine the relative difference in the response of the power meter at those two power levels. By making many of these measurements over the entire dynamic range of the power meter, a dynamic calibration curve can be generated.

The calibration curve is obtained by relating the true optical power P_{true} to the measured power V at some range setting R as a polynomial of order n with coefficients $b_{R,k}$:

$$P_{\text{true}} = Ca_R\left(V + \sum_{k=2}^{n} b_{R,k}V^k\right), \tag{1}$$

where a_R is a scale factor applying to the entire range R, and C is the absolute calibration factor of the power meter at the reference power level. Optical power V_1 is then measured while shutter 2 is closed, V_2 is measured with shutter 1 closed, and V_3 is measured with both shutters open. Assuming the relationship (1) between measured and true power, we obtain the equivalence

$$\left(V_3 - V_1 - V_2\right) + \sum_{k=2}^{n} b_{R,k}\left(V_3^k - V_1^k - V_2^k\right) = 0. \tag{2}$$

The dynamic calibration curve for a given range setting is arrived at by making many such measurements and determining the coefficients $b_{R,k}$ by a least-squares fit. Separate ranges are related to each other by making multiple equal-power measurements at different range settings, which solves for the variables a_R. The result is a full dynamic calibration curve. Two such examples of dynamic calibration curves for an HP81524A InGaAs detector, 5 mm$\times$5 mm area, are shown in Fig. 6 (1550 nm) and Fig. 7 (860 nm). The flatness of the calibration curve at 1550 nm may be due to the optimization of the power meter for operation at wavelengths near 1550 nm.

As can be seen in Fig. 7 the 860 nm responsivity of this power meter at an illumination power of -50 dBm is about 0.6 % lower than at 0 dBm. The detection efficiency measurement shown in Fig. 4 is accomplished at these two power levels. As an example of the importance of measuring the calibration curve of the power meter, we note that omitting this correction would result in an overestimate of the device efficiency by 1.8 % (absolute percent). This error is on order of the total loss of our detection system and, therefore, careful consideration must

#143645 - $15.00 USD
Received 8 Mar 2011; accepted 25 Mar 2011; published 25 Apr 2011

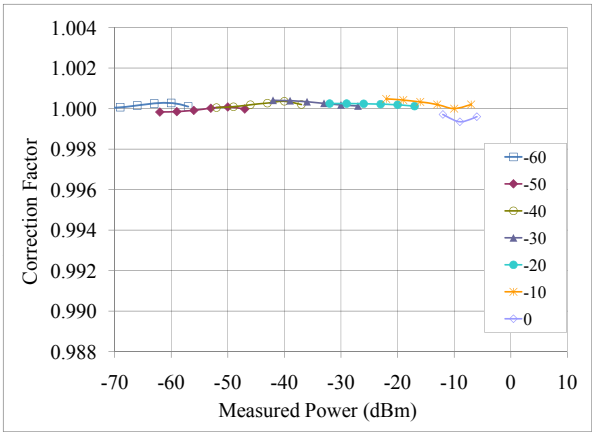

Fig. 6. Example dynamic calibration curves for a wavelength of 1550 nm. Calibrated input power levels are given by (measured power)/(correction factor).

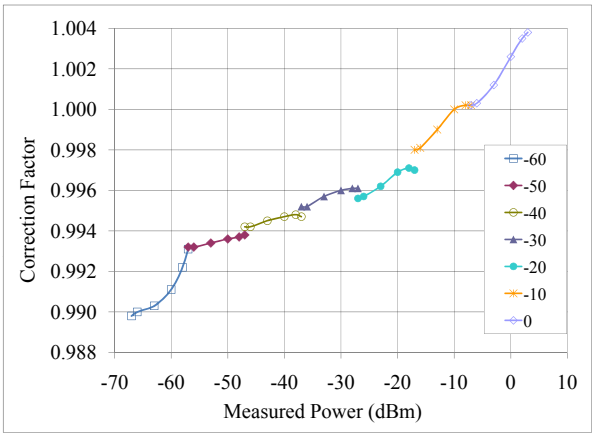

Fig. 7. Example dynamic calibration curves for a wavelength of 860 nm. Calibrated input power levels are given by (measured power)/(correction factor).

be given to the power meter calibration factors when one is measuring near-unity efficiency single-photon detectors. The efficiency of each device was measured by use of a 5–10 % duty cycle pulsed diode laser source at the design wavelength of each device. The use of a pulsed source eliminates the pileup-related counting errors associated with a continuous (CW) detection efficiency measurement. The electrical current through the TES device is amplified using a cryogenic SQUID amplifier followed by room-temperature amplification and pulse shaping (filtering). The resulting signal is processed and accumulated by a multichannel analyzer [3]. After applying the proper corrections to the measured count rate for a given source flux, we find extremely high system detection efficiency and excellent reproducibility across device assemblies. Figure 8 shows results obtained for devices optimized for high efficiency at wavelengths of 805 nm, 850 nm, and 1550 nm. This figure contains data from all devices calibrated with this method and is not the result of rejecting low-performing outliers. The reproducibility of the measured efficiencies within each batch of detectors ($1\ \sigma \approx\ 2$ %) represents a worst-case measurement of the reproducibility of the alignment technique. Including the back-reflection measurements and optical modeling, however, we have confidence that the coupling efficiency

#143645 - $15.00 USD
Received 8 Mar 2011; accepted 25 Mar 2011; published 25 Apr 2011

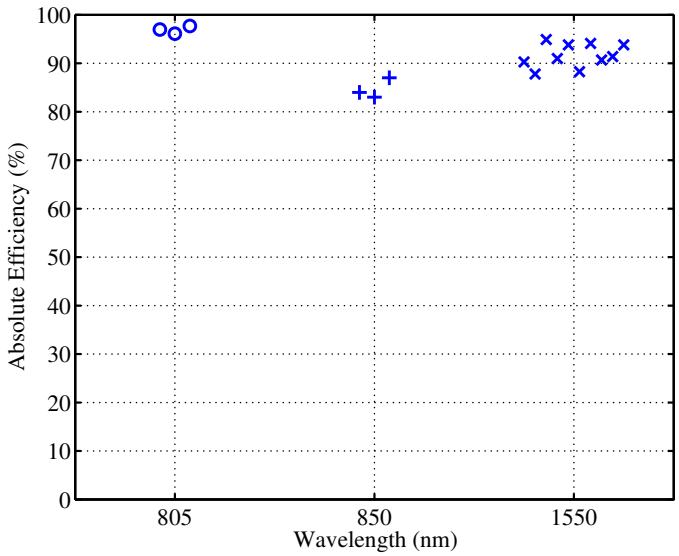

Fig. 8. System detection efficiency results in absolute percent for self-aligned TES devices from four separate wafer fabrication runs. Devices are optimized for optimal efficiency at a wavelength of 805 nm (○), 850 nm (+), and 1550 nm (×). Points at each wavelength are arbitrarily offset horizontally for clarity. Efficiency measurements were made using pulsed diode laser sources at the design wavelength of each device.

is greater than 99 % and the measured variance in system detection efficiency is dominated by (unmeasured) variability in fiber splice loss and device absorption efficiency. Work is in progress to quantify these system losses *in situ*.

5. Conclusion

The nearly lossless, self-aligning fiber-to-detector coupling method described in this paper has been demonstrated to be reproducible, cryogenically stable, and simple to assemble, and is now used as our primary fiber-coupling method for high-efficiency photon-number resolving devices. The single-photon-level detector calibration scheme has enabled the demonstration of a robust, self-aligning packaging technique that shows no indication of alignment drift across multiple warm-up/cool-down cycles for a packaged device. We expect this technique to gain widespread adoption for the low-loss coupling of optical fibers to cryogenic devices.

Acknowledgments

This work was supported by the NIST Quantum Information Initiative and the Albion College Faculty Development Fund. The authors are grateful to Daniel Schmidt at NIST for his assistance in photographing our assemblies, Marty Gould for machining and mechanical advice and Jeff VanLanen for aid in implementing many of the techniques presented. This work is a contribution of the US Government and is not subject to US Copyright.